ZVS-Optimized Constant and Variable Switching Frequency Modulation Schemes for Dual Active Bridge Converters

Lyu, Dingsihao; Straathof, Coen; Soeiro, Thiago Batista; Qin, Zian; Bauer, Pavol

DOI
10.1109/OJPEL.2023.3319970

Publication date
2023

Document Version
Final published version

Published in
IEEE Open Journal of Power Electronics

IEEE Open Journal of
Power Electronics

Received 7 August 2023; revised 19 September 2023; accepted 23 September 2023. Date of publication 27 September 2023; date of current version 11 October 2023. The review of this article was arranged by Associate Editor Lijun (GAE | OJ GE) Hang.

Digital Object Identifier 10.1109/OJPEL.2023.3319970

ZVS-Optimized Constant and Variable Switching Frequency Modulation Schemes for Dual Active Bridge Converters

DINGSIHAO LYU [1] (Graduate Student Member, IEEE), COEN STRAATHOF [2], THIAGO BATISTA SOEIRO [3] (Senior Member, IEEE), ZIAN QIN [4] (Senior Member, IEEE), AND PAVOL BAUER [4] (Senior Member, IEEE)

[1]EEMCS, Delft University of Technology, 2628 CD Delft, The Netherlands
[2]EST Floattech, 1171 PL Badhoevedorp, The Netherlands
[3]EEMCS, University of Twente, 7522 NB Enschede, The Netherlands
[4]EEMCS, Delft University of Technology, 2628 CD Delft, The Netherlands

CORRESPONDING AUTHOR: DINGSIHAO LYU (e-mail: d.lyu@tudelft.nl)

This work was supported by European H2020 Research and Innovation Program, ECSEL Joint Undertaking, and National Funding Authorities from eight participating countries, such as Austria, Finland, Germany, including the Free States of Saxony and Thuringia, Hungary, The Netherlands, Slovakia, Spain, and Switzerland under Grant 826417.

ABSTRACT This paper proposes two modulation schemes for Dual Active Bridge (DAB) converters, with the aim of maximizing Zero Voltage Switching (ZVS) operation over a wide operational range. The first is a ZVS-optimized constant frequency modulation scheme, constructed based on the boundary conditions of ZVS operation. This scheme maximizes the number of ZVS events across a broad operational range and is easy to implement. Additionally, a variable frequency modulation scheme is proposed, enabling continuous full ZVS operation for the DAB converter at full power and eliminating the loss of ZVS due to transitioning between modulation regions. This functionality extends the full ZVS range, yielding improved Electromagnetic Interference (EMI) performance and overall power efficiency. The synergy of the proposed modulation schemes is particularly well-suited for applications like off-board Electric Vehicle (EV) charging. Experimental validation, conducted on an 11-kW DAB converter prototype with an output voltage range of 250 V to 950 V, demonstrates the efficacy of the proposed schemes in achieving ZVS and boosting converter efficiency.

INDEX TERMS Dual active bridge, ZVS, soft switching, EV charging, wide voltage range.

I. INTRODUCTION

The dual-active-bridge (DAB) converter is firstly proposed in [1], [2] as a soft switching DC/DC converter suitable for high power applications, and studies have been conducting ever since to improve its performance [3], [4], [5], [6], [7], [8], [9], [10], [11], [12], [13], [14], [15], [16], [17], [18], [19], [20], [21], [22], [23], [24], [25], [26], [27], [28], [29], [30], [31], [32], [33], [34], [35], [36], [37], [38], [39]. The DAB converter consists of two H-bridges, with a transformer that has a relatively large leakage inductance L, as shown in Fig. 1(a). Each half-bridge in the circuit operates up to a 50% duty cycle. There are four control parameters that can be manipulated to control the DAB converter. Namely, the phase shift Φ between the two H-bridges, the effective duty cycle of the left and right H-bridge $D_{1,2}$, and the switching frequency f_{sw}. These parameters are depicted in the typical operational waveform shown in Fig. 1(b)–(i).

Due to its advantages of small number of components, zero voltage switching (ZVS) ability, buck-boost operation, and bidirectional power flow, The DAB converter is obtaining attention progressively in the electric vehicle (EV) charging application [21], [23], [27], [28], [35].

Most EVs launched last decade have a nominal battery voltage of around 400 V. Currently, high-end EV manufacturers are increasingly adopting 800 V battery architectures due to their benefits: reduced vehicle weight and faster battery

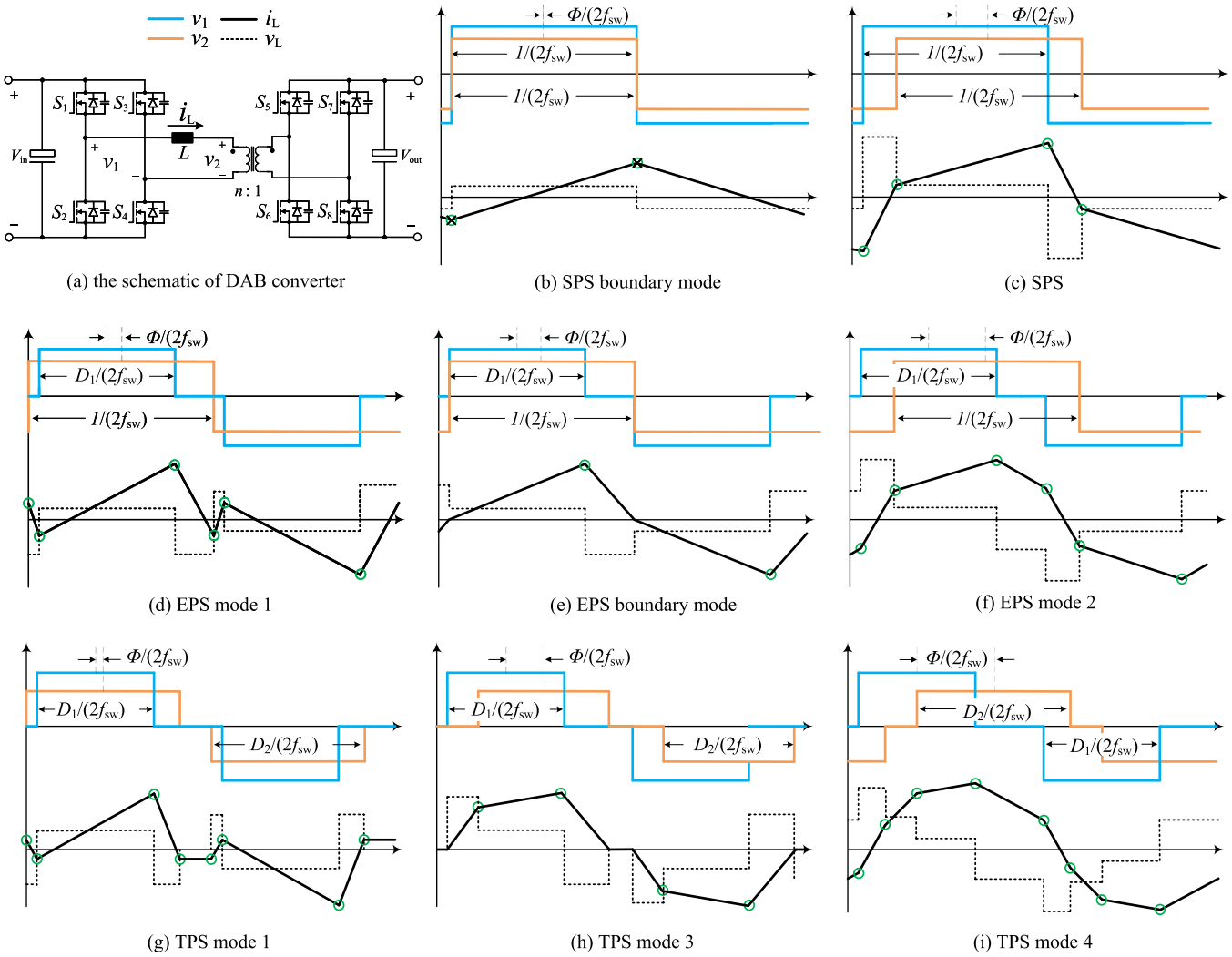

(a) the schematic of DAB converter (b) SPS boundary mode (c) SPS

(d) EPS mode 1 (e) EPS boundary mode (f) EPS mode 2

(g) TPS mode 1 (h) TPS mode 3 (i) TPS mode 4

FIGURE 1. Schematics of the DAB converter and the typical operational waveform of SPS (c), EPS (d), (f), TPS (g), (h), (i) modulation in the advantageous modes, and two boundary modes denoted as SPS transition mode (b) and EPS transition mode (e).

charging times using public DC-fast charging infrastructures. This is especially advantageous as public charger cable current ratings are limited by thermal management. Therefore, today the public DC-type EV charging infrastructures should be able to supply power efficiently to both 400 V and 800 V EV battery classes.

One of the main challenges for the DAB converter in the public EV charging application is maintaining the high-efficiency performance and zero voltage switching (ZVS) ability in an extended power and voltage regulation range. The conventional single phase shift (SPS) modulation method is the simplest modulation method, which regulates the voltage and power level by controlling Φ [1], [2], [3]. At unity voltage gain scenarios, the SPS modulation can provide ZVS over most of the operating range. Fig. 1(c) shows the typical operational waveform of the SPS modulation method where all transistors operate in ZVS turn-on.

However, at non-unity voltage gain scenarios, the ZVS range is limited at light loads, and current stress is high compared to more advanced modulation methods [3], [4], [5], [6], [7], [8], [9], [11], [12], [13], [14], [15], [19], [20], [22], [23], [24], [25], [26], [28], [29], [31], [32], [33], [34], [35]. Fig. 1(b) shows the waveform of an extreme mode of the SPS modulation, herein denoted as the SPS transition mode, where the operating power and Φ are close to zero. It can be seen that 4 out of 8 transistors lose ZVS. In order to enlarge the ZVS range and reduce the current stress of the SPS modulation especially in the light to medium load and non-unity voltage gain scenarios, the control parameters $D_{1,2}$ are introduced into the modulation methods. As a result, the extended phase shift (EPS) modulation, the dual phase shift (DPS) modulation and the triple phase shift (TPS) modulation are investigated.

The DPS modulation of DAB converter is introduced In [7] to eliminate reactive power in light load operations. The DPS adjusts D_1 and D_2 ($D_1 = D_2$) between 0% and 100% while controlling Φ. It offers wider power transmission and more power transfer than SPS with the same Φ and current stress as per [20]. [33] identifies four DPS modulation modes and proposes an optimized scheme using magnetizing current.

However, [30] suggests that DPS is generally inferior to EPS due to higher current stress.

The EPS mode 2 modulation, as proposed in [5], extends the soft switching range of the DAB converter by adjusting Φ and D_1/D_2 based on the largest DC voltage. Although it enhances the ZVS range, it encounters hard-switching issues under light loads. Subsequent works have optimized and extended its soft switching capabilities, with EPS mode 1 enabling ZVS even in light load scenarios where EPS mode 2 fails [6], [12]. The asymmetric EPS modulation introduces a DC offset, necessitating a blocking capacitor [29]. Finally, the studies in [31], [32] employ magnetizing current to further extend the ZVS range, but this approach leads to sub-optimal transformer design and elevated current stresses.

Among TPS, EPS, and DPS, TPS is the most versatile modulation method, permitting independent control of all three parameters: Φ and $D_{1/2}$. EPS and DPS are derivatives of TPS, designed to minimize complexity. Out of the twelve identified TPS modes, due to symmetry, only five warrant examination [11], [13], [19], [24], [26]. These are labeled as TPS mode 1 to 5 [19], [26]. TPS modes 2 and 5 have been demonstrated to be disadvantageous [11], [13] due to their lack of ZVS ability and elevated current stresses. As a result, numerous modulation schemes in literature utilize TPS mode 1, 3, and 4 [11], [13], [19], [24], [26]. Fig. 1(g)–(i) depict the typical waveforms of TPS mode 1, 3, and 4, respectively. It is evident that EPS mode 1 is a specific case of TPS mode 1, while EPS mode 2 is a specific case of TPS mode 4.

Several researchers have proposed distinctive modulation schemes that amalgamate modulation methods to optimize efficiency performance for DAB converters relative to SPS modulation. The authors of [4], [9] recommend a blend of triangular (a boundary case between TPS mode 1 and 3) and trapezoidal (a specialized case of TPS mode 3) current modulation for optimal system efficiency. However, only four and two out of eight transistors can achieve ZVS in trapezoidal and triangular modes, respectively, with the remaining transistors only achieving Zero Current Switching (ZCS). In [11], to extend the soft-switching range to the zero-load condition and to reduce rms and peak currents, the recommendation is to operate in TPS mode 1 at low power due to its full ZVS ability and concurrently minimized rms current, and in EPS mode 2 (a special case of TPS mode 4) at high power. At maximum power, EPS mode 2 naturally transitions into SPS. However, the analysis of the critical ZVS condition is not accurate, as it overlooks the output capacitance of the transistors. This omission can result in sub-optimal ZVS performance during practical implementation. To mitigate the conduction and copper losses, [13] employs TCM (TPS mode 3) for low power, OTM (TPS mode 4) for medium power, and CPM (SPS) for high power, even though some switches do not achieve ZVS in TPS mode 3. Additionally, the formulation of the modulation scheme is intricate for practical implementation. The studies in [19], [24], [26] optimize current stress using varying combinations of EPS and TPS modes. [28] employs SPS for heavy loads and transitions to EPS2, EPS1, and TPS1 as the load decreases. However, implementing the transition between the nine modulation modes using a state machine is not straightforward, and the ZVS loss during the transition is not thoroughly explored. [35] introduces a modulation scheme for DAB converters that maximizes the ZVS range and achieves quasi-optimal inductor rms current, amalgamating TPS1, EPS1, EPS2, and SPS. In [36], universal analytical expressions for TPS modulation are derived, and an RMS current-minimized scheme, grounded in GOC equations, is introduced. However, it prioritizes RMS current reduction, potentially compromising optimal ZVS performance. Asymmetric duty modulation, explored in [37], [38], provides additional flexibility through duty cycle adjustments, resulting in reduced RMS current and an expanded soft-switching range. However, its complexity, compared to symmetrical duty modulations, poses challenges to implementation. The ZVS analysis in [38], based on the stored energy equation, omits energy considerations from the non-switching bridge, leading to inaccuracies acknowledged by the authors. Although [38] demonstrates full ZVS operation, it is confined to BUCK mode operation with a voltage regulation range from 0.5 to 1.

Component modifications and variable switching frequency modulation have also been explored in the literature to enhance the DAB converter's performance. [10] employs variable AC link reactance with a dual leakage transformer to mitigate peak transformer currents during light load SPS operation. [22] introduces a modulation scheme utilizing a voltage offset across the DC blocking capacitor, allowing for a broader soft-switching range with simple implementation. Expanding the ZVS range by decreasing magnetizing inductance is also possible [32], [33], [40]. However, these methods require hardware changes, such as specific transformer designs and additional capacitors, possibly reducing power density and increasing current stress. An alternative is to manipulate the switching frequency without hardware alterations. [17] proposes finding the optimal design trade-off among switching loss, conduction loss, and drive loss by manipulating the switching frequency. However, the possibility of maximizing the ZVS range is not explored. The work in [18], [20] proposes including variable switching frequency in SPS and EPS modulation to extend the soft-switching range. However, the ZVS analysis is based on inductive and capacitive energy equations, which are inaccurate due to the omission of energy provided by the non-switching bridge.

In conclusion, compared to the operation with only SPS method, an appropriate modulation scheme, comprising SPS, DPS, EPS, and TPS methods significantly enlarges the ZVS range and reduces current stress in the DAB converter. However, it is still challenging to achieve a full ZVS operation in a wide voltage regulation range application such as EV charging due to the inevitable ZVS lost during the transition between these modulation methods. Most of the proposed modulation schemes in the literature focus on the optimization of current stresses, leading to sub-optimal ZVS performance. And the modulation scheme are practically hard to implement.

Moreover, there is no study covering the wide voltage range operation of the DAB converter from 250 V to 1000 V, which is necessary for the off-board EV charging application.

In the context of EV charging applications, converters or power modules are expected to operate at full power for the majority of charging scenarios, particularly in common situations such as home charging and workplace charging [41]. In these scenarios, low to medium power chargers with a capacity of up to 50 kW are commonly used, and they operate at their full power until the batteries of the EVs reach a high state of charge (SOC). This behavior is evident in charging profiles from various sources such as [42], [43], [44], where 50 kW chargers continue to operate at full power until the EV's SOC exceeds 80%. In fast to ultra-fast charging scenarios, the individual power modules within the charger also operate at full power most of the time, particularly when implementing the multi-step constant current (MSCC) charging strategy [45]. Under this strategy, power modules run at full power until the required charging power decreases, at which point they are sequentially turned off. Charging profiles from sources like [46], [47], [48], [49] exemplify these charging scenarios. Consequently, operating with a reduced number of ZVS events at full power operating points is undesirable due to its adverse effects on both Electromagnetic Interference (EMI) performance and power efficiency. It is crucial to achieving continuous ZVS operation for minimizing the switch-bridge cross-talk caused by the hard switching and achieving high efficiency performance throughout the charging process.

This paper proposes to combine the TPS mode 1, EPS mode 1, EPS mode 2 together to form a ZVS-advantageous constant switching frequency modulation scheme. These three modes are chosen because their operational ranges are naturally connected, meaning there will not be any abrupt change of phase shifts during the changing of modes. With this modulation scheme, the DAB converter is able to operate with full ZVS for all eight switches in most of the operational points. However, two or four out of eight switches can lose ZVS during the transition region where the DAB changes between the EPS mode 1 and 2. To address this issue, for the dominating full power charging scenarios, the variable switching frequency is introduced into the modulation scheme to ensure full ZVS performance. Since in the EV charging application, the converter will operate in full power condition most of the time, this modulation scheme will ensure reliable operation of the EV charger without introducing modification on the converter components or topology.

The main contributions of this paper are as follows:

- The proposal of a ZVS-optimized constant frequency modulation scheme and its construction method based on straightforward ZVS analysis. The proposed scheme aims to maximize ZVS events in the DAB converter while ensuring easy practical implementation.
- The proposal of a variable switching frequency modulation scheme and its construction method to address the lost of ZVS issue during mode transition in the constant frequency modulation scheme. This variable switching frequency modualtion scheme ensures full ZVS operation of the DAB converter in a wide voltage range during the full power charging process to improve the EMI performance.
- The experimental testing of the proposed modulation schemes on an 11 kW DAB prototype with a wide output voltage range (250–950 V). This wide voltage range test of the DAB converter was not yet elaborated on in the literature. This is particularly important because it demonstrates the feasibility of the proposed modulation schemes for the future EV market.

This paper is arranged as follows. In Section II, the analytical expressions of the DAB converter in TPS mode 1 and 4 are introduced, including the operational conditions of $D_1/D_2/\Phi$, the calculations of inductor current i_L values, and the ZVS requirements for different switching actions. The boundary conditions to operate with full ZVS for all eight switches are derived based on the analytical current calculation and the general ZVS requirements. Section III presents the proposed ZVS-optimized constant frequency modulation scheme and the analytical method to construct it. Moreover, the issue of the ZVS lost during the transition of modulation methods is explained in detail. Section IV presents the proposed variable switching frequency modulation scheme and the method of its construction. In Section V, the modulation schemes are tested on a DAB prototype, and the results are presented. The ZVS and efficiency performance of the proposed modulation scheme are verified and compared. The conclusion is presented in Section VI.

II. ANALYTICAL EXPRESSIONS OF THE TPS MODE 1 AND 4

The EPS mode 1 and 2 modulations are special cases of TPS mode 1 and 4 modulations, which can be observed in Fig. 1. Thus, the analyses of TPS mode 1 and 4 are presented in this paper as they are more general and cover the cases for EPS mode 1 and 2. In order to be categorized into TPS mode 1 and 4 as shown in Fig. 1(g) and (i), the values of the phase shifts need to fall within the operational conditions summarized in Table 1.

For the SPS, TPS mode 1, and mode 4, two types of switching actions occur, the switching of a switching leg (a half-bridge), and the switching of a H-bridge. When the switching action of a half-bridge happens, the voltage of that H-bridge will change between zero and $\pm V$. And when the switching action of a H-bridge happens, the voltage of it will change between $+V$ and $-V$. Table 2 summarised the analytical expressions for the instantaneous current values of i_L at each switching action.

According to the different voltage changes, the general ZVS requirements for the switching actions are summarized in Table 3. Z is the characteristic impedance of the LC resonant circuitry during the half-bridge switching actions, and it can be calculated by (1).

$$Z = \sqrt{\frac{L}{2C_{oss}}} \tag{1}$$

TABLE 1. The Operational Range and the Power Calculation Equations of the TPS Mode 1 and 4

TPS	operational conditions	power
mode 1	$\lvert D_1 - D_2\rvert \geq 2\lvert\Phi\rvert$	$\frac{D_1\Phi V_{\text{in}} n V_{\text{out}}}{2Lf_{\text{sw}}}$, if $V_{\text{in}} \geq nV_{\text{out}}$
	$\text{sgn}(D_2 - D_1) = \text{sgn}(V_{\text{in}} - nV_{\text{out}})$	$\frac{D_2\Phi V_{\text{in}} n V_{\text{out}}}{2Lf_{\text{sw}}}$, if $V_{\text{in}} < nV_{\text{out}}$
mode 4	$D_1 + D_2 \geq 2\lvert\Phi\rvert$ $D_1 + D_2 \geq 2 - 2\lvert\Phi\rvert$	$\text{sgn}(\Phi)\frac{-(D_1^2+D_2^2+4\lvert\Phi\rvert^2-2D_1-2D_2-4\lvert\Phi\rvert+2)V_{\text{in}} n V_{\text{out}}}{8Lf_{\text{sw}}}$

TABLE 2. The Steady State Analytical Expressions of i_{L} Values for $\Phi > 0$

modulation		switching	i_{L} values
SPS		$v_1 : +V_{\text{in}} \to -V_{\text{in}}$	$\frac{V_{\text{in}}+(2\Phi-1)nV_{\text{out}}}{4Lf_{\text{sw}}}$
		$v_2 : -nV_{\text{out}} \to +nV_{\text{out}}$	$\frac{nV_{\text{out}}+(2\Phi-1)V_{\text{in}}}{4Lf_{\text{sw}}}$
TPS mode 1	$V_{\text{in}} \geq nV_{\text{out}}$	$v_2 : 0 \to +nV_{\text{out}}$	$\frac{D_2 nV_{\text{out}}-D_1V_{\text{in}}}{4Lf_{\text{sw}}}$
		$v_1 : 0 \to +V_{\text{in}}$	$\frac{(2\Phi+D_1)nV_{\text{out}}-D_1V_{\text{in}}}{4Lf_{\text{sw}}}$
		$v_1 : +V_{\text{in}} \to 0$	$\frac{(2\Phi-D_1)nV_{\text{out}}+D_1V_{\text{in}}}{4Lf_{\text{sw}}}$
		$v_2 : +nV_{\text{out}} \to 0$	$\frac{D_1V_{\text{in}}-D_2nV_{\text{out}}}{4Lf_{\text{sw}}}$
	$V_{\text{in}} < nV_{\text{out}}$	$v_1 : 0 \to +V_{\text{in}}$	$\frac{D_2 nV_{\text{out}}-D_1V_{\text{in}}}{4Lf_{\text{sw}}}$
		$v_2 : 0 \to +nV_{\text{out}}$	$\frac{(2\Phi-D_2)V_{\text{in}}+D_2nV_{\text{out}}}{4Lf_{\text{sw}}}$
		$v_2 : +nV_{\text{out}} \to 0$	$\frac{(2\Phi+D_2)V_{\text{in}}-D_2nV_{\text{out}}}{4Lf_{\text{sw}}}$
		$v_1 : +V_{\text{in}} \to 0$	$\frac{D_1V_{\text{in}}-D_2nV_{\text{out}}}{4Lf_{\text{sw}}}$
TPS mode 4		$v_1 : 0 \to +V_{\text{in}}$	$-\frac{D_1V_{\text{in}}+(2\lvert\Phi\rvert+D_1-2)nV_{\text{out}}}{4Lf_{\text{sw}}}$
		$v_2 : -nV_{\text{out}} \to 0$	$\frac{(2\lvert\Phi\rvert+D_2-2)V_{\text{in}}+D_2nV_{\text{out}}}{4Lf_{\text{sw}}}$
		$v_2 : 0 \to +nV_{\text{out}}$	$\frac{(2\lvert\Phi\rvert-D_2)V_{\text{in}}+D_2nV_{\text{out}}}{4Lf_{\text{sw}}}$
		$v_1 : +V_{\text{in}} \to 0$	$\frac{D_1V_{\text{in}}-(D_1-2\lvert\Phi\rvert)nV_{\text{out}}}{4Lf_{\text{sw}}}$

TABLE 3. The ZVS Requirements on i_{L} for Different Switching Actions. V_1 and V_2 Here are the Voltage Value of v_1 and v_2 At the Switching Actions

switching actions	conditions	i_{L} requirement
$v_1 : 0 \to +V_{\text{in}}$	if $V_2 < V_{\text{in}}/2$	$\leq -\frac{V_{\text{in}}\sqrt{1-2V_2/V_{\text{in}}}}{Z}$
	if $V_2 \geq V_{\text{in}}/2$	≤ 0
$v_1 : +V_{\text{in}} \to 0$	if $V_2 > V_{\text{in}}/2$	$\geq -\frac{V_{\text{in}}\sqrt{1-2V_2/V_{\text{in}}}}{Z}$
	if $V_2 \leq V_{\text{in}}/2$	≥ 0
$v_1 : 0 \to -V_{\text{in}}$	if $V_2 > -V_{\text{in}}/2$	$\geq \frac{V_{\text{in}}\sqrt{1+2V_2/V_{\text{in}}}}{Z}$
	if $V_2 \leq -V_{\text{in}}/2$	≥ 0
$v_1 : -V_{\text{in}} \to 0$	if $V_2 < -V_{\text{in}}/2$	$\leq \frac{V_{\text{in}}\sqrt{1+2V_2/V_{\text{in}}}}{Z}$
	if $V_2 \geq -V_{\text{in}}/2$	≤ 0
$v_1 : +V_{\text{in}} \to -V_{\text{in}}$	if $V_2 > 0$	$\geq \frac{V_{\text{in}}\sqrt{8V_2/V_{\text{in}}}}{Z}$
	if $V_2 \leq 0$	≥ 0
$v_1 : -V_{\text{in}} \to +V_{\text{in}}$	if $V_2 < 0$	$\leq \frac{V_{\text{in}}\sqrt{8V_2/V_{\text{in}}}}{Z}$
	if $V_2 \geq 0$	≤ 0
$v_2 : 0 \to +nV_{\text{out}}$	if $V_1 < nV_{\text{out}}/2$	$\geq \frac{nV_{\text{out}}\sqrt{1-2V_1/(nV_{\text{out}})}}{Z/n}$
	if $V_1 \geq nV_{\text{out}}/2$	≥ 0
$v_2 : +nV_{\text{out}} \to 0$	if $V_1 > nV_{\text{out}}/2$	$\leq \frac{nV_{\text{out}}\sqrt{1-2V_1/(nV_{\text{out}})}}{Z/n}$
	if $V_1 \leq nV_{\text{out}}/2$	≤ 0
$v_2 : 0 \to -nV_{\text{out}}$	if $V_1 > -nV_{\text{out}}/2$	$\leq -\frac{nV_{\text{out}}\sqrt{1+2V_1/(nV_{\text{out}})}}{Z/n}$
	if $V_1 \leq -nV_{\text{out}}/2$	≤ 0
$v_2 : -nV_{\text{out}} \to 0$	if $V_1 < -nV_{\text{out}}/2$	$\geq -\frac{nV_{\text{out}}\sqrt{1+2V_1/(nV_{\text{out}})}}{Z/n}$
	if $V_1 \geq -nV_{\text{out}}/2$	≥ 0
$v_2 : +nV_{\text{out}} \to -nV_{\text{out}}$	if $V_1 > 0$	$\leq -\frac{nV_{\text{out}}\sqrt{8V_1/(nV_{\text{out}})}}{Z/n}$
	if $V_1 \leq 0$	≤ 0
$v_2 : -nV_{\text{out}} \to +nV_{\text{out}}$	if $V_1 < 0$	$\geq -\frac{nV_{\text{out}}\sqrt{8V_1/(nV_{\text{out}})}}{Z/n}$
	if $V_1 \geq 0$	≥ 0

For the deriving of the expressions in Table 3, the conventional inductive and capacitive stored energy equation for ZVS analysis are used by numerous papers [18], [20], [38]. It is usually written as $0.5LI^2 > 0.5nC_{\text{oss}}V_{\text{ds}}^2$, in which L is the leakage or external inductance value, and n is the number of transistors involved during the switching transition. This equation oversimplifies the energy exchange during the switching transition because it ignores the energy provided by the non-switching bridge, leading to inaccurate ZVS analysis. In this paper that energy is taken into consideration. As shown from the ZVS conditions listed in Table 3 , the ZVS current requirement expressions include the non-switching bridge voltage as well.

Combining the current values and the ZVS requirements for the switching actions, sets of inequations can be derived to ensure ZVS at each switching action. The boundary conditions for the DAB converter to operate with full ZVS for all eight switches can be derived for different modulation methods based on these sets of equations.

A. FULL ZVS BOUNDARY CONDITIONS FOR TPS MODE 1

When $V_{\text{in}} > nV_{\text{out}}$ Combining the current values and the ZVS requirements for the three switching actions, ($v_2 : 0 \to +nV_{\text{out}}$), ($v_1 : 0 \to +V_{\text{in}}$), ($v_1 : +V_{\text{in}} \to 0$), the following inequation system can be derived for ensuring the full ZVS performance.

$$\frac{D_2 nV_{\text{out}} - D_1V_{\text{in}}}{4Lf_{\text{sw}}} \geq \frac{nV_{\text{out}}}{Z/n} \tag{2}$$

$$\frac{(2\Phi + D_1)nV_{\text{out}} - D_1V_{\text{in}}}{4Lf_{\text{sw}}} \leq -\frac{V_{\text{in}}\sqrt{1-2k}}{Z}, k_{\text{w}} = 0 \tag{3}$$

$$\frac{(2\Phi - D_1)nV_{\text{out}} + D_1V_{\text{in}}}{4Lf_{\text{sw}}} \geq \frac{V_{\text{in}}\sqrt{2k-1}}{Z}, k_{\text{w}} = 1 \tag{4}$$

k is defined as the voltage ratio as in (5), and k_w is the worst case value of k.

$$k = \frac{nV_{\text{out}}}{V_{\text{in}}} \tag{5}$$

Substituting k using the worst value k_{w} in this equation system, the following boundary conditions can be derived:

$$D_1 \geq \frac{2k|\Phi|}{1-k} + \frac{4Lf_{\text{fw}}}{Z(1-k)} \tag{6}$$

$$D_2 \geq \frac{2|\Phi|}{1-k} + \frac{4Lf_{\text{fw}}}{Zk(1-k)} + \frac{4Lf_{\text{fw}}}{Z/n} \tag{7}$$

Since D_2 is always larger than D_1 when $V_{\text{in}} > nV_{\text{out}}$, The value of Φ allowed for the equation system to hold true can be calculated by solving the following equation:

$$D_2 = \frac{2|\Phi|}{1-k} + \frac{4Lf_{\text{fw}}}{Zk(1-k)} + \frac{4Lf_{\text{fw}}}{Z/n} \leq 1 \tag{8}$$

Solving this equation, the boundary condition for the value of Φ can be derived as (9). And the maximum value of Φ for the converter to operate in the TPS mode 1 modulation, $\Phi_{\text{TPS(max)}}$, can also be obtained from (9).

$$|\Phi| \leq \frac{1-k}{2} - \frac{2Lf_{\text{sw}}}{Zk} - \frac{2Lf_{\text{sw}}n(1-k)}{Z} \tag{9}$$

When $V_{\text{in}} < nV_{\text{out}}$ Similarly, the following equation system can be derived for ensuring the full ZVS performance of the TPS mode 1 modulation when $V_{\text{in}} < nV_{\text{out}}$.

$$\frac{D_2nV_{\text{out}} - D_1V_{\text{in}}}{4Lf_{\text{sw}}} \leq -\frac{V_{\text{in}}}{Z} \tag{10}$$

$$\frac{(2\Phi - D_2)V_{\text{in}} + D_2nV_{\text{out}}}{4Lf_{\text{sw}}} \geq \frac{nV_{\text{out}}\sqrt{1-2k^{-1}}}{Z/n}, k_{\text{w}}^{-1} = 0 \tag{11}$$

$$\frac{(2\Phi + D_2)V_{\text{in}} - D_2nV_{\text{out}}}{4Lf_{\text{sw}}} \leq -\frac{nV_{\text{out}}\sqrt{2k-1}}{Z/n}, k_{\text{w}}^{-1} = 1 \tag{12}$$

Based on this inequation system, the following boundary conditions can be derived:

$$D_2 \geq \frac{2k^{-1}|\Phi|}{1-k^{-1}} + \frac{4Lf_{\text{sw}}n}{Z(1-k^{-1})} \tag{13}$$

$$D_1 \geq \frac{2|\Phi|}{1-k^{-1}} + \frac{4Lf_{\text{sw}}n}{Zk^{-1}(1-k^{-1})} + \frac{4Lf_{\text{sw}}}{Z} \tag{14}$$

$$|\Phi| \leq \frac{1-k^{-1}}{2} - \frac{2Lf_{\text{sw}}n}{Zk^{-1}} - \frac{2Lf_{\text{sw}}(1-k^{-1})}{Z} \tag{15}$$

B. FULL ZVS BOUNDARY CONDITIONS FOR EPS MODE 2

When $V_{\text{in}} > nV_{\text{out}}$ Combining the current values and the ZVS requirements for the three switching actions, ($v_1 : 0 \rightarrow +V_{\text{in}}$), ($v_2 : -nV_{\text{out}} \rightarrow +nV_{\text{out}}$), ($v_1 : +V_{\text{in}} \rightarrow 0$), the following equation system can be derived for ensuring the full ZVS performance.

$$\frac{(2-2|\Phi|-D_1)nV_{\text{out}} - D_1V_{\text{in}}}{4Lf_{\text{sw}}} \leq -\frac{V_{\text{in}}\sqrt{1+2k}}{Z}, k_{\text{w}} = 1 \tag{16}$$

$$\frac{(2|\Phi|-1)V_{\text{in}} + nV_{\text{out}}}{4Lf_{\text{sw}}} \geq 0 \tag{17}$$

$$\frac{D_1V_{\text{in}} + (2|\Phi|-D_1)nV_{\text{out}}}{4Lf_{\text{sw}}} \geq \frac{V_{\text{in}}\sqrt{2k-1}}{Z}, k_{\text{w}} = 1 \tag{18}$$

Based on this equation system, the following boundary conditions can be derived, and the minimum value of D and Φ for the DAB converter to operate in the EPS mode 2 modulation with full ZVS, $D_{\text{EPS2(min)}}$ and $\Phi_{\text{EPS2(min)}}$, can also be calculated.

$$D_1 \geq \frac{(2-2|\Phi|)k + (4\sqrt{3}Lf_{\text{sw}})/Z}{1+k} \tag{19}$$

$$D_1 \geq \frac{-2|\Phi|k + (4Lf_{\text{sw}})/Z}{1-k} \tag{20}$$

$$|\Phi| \geq 0.5 - 0.5k \tag{21}$$

When $V_{\text{in}} < nV_{\text{out}}$

$$\frac{(2|\Phi|-1)nV_{\text{out}} + V_{\text{in}}}{4Lf_{\text{sw}}} \geq \frac{nV_{\text{out}}\sqrt{8k^{-1}}}{Z}, k_{\text{w}} = 1 \tag{22}$$

$$\frac{D_2nV_{\text{out}} + (2|\Phi| + D_2 - 2)V_{\text{in}}}{4Lf_{\text{sw}}} \geq \frac{nV_{\text{out}}\sqrt{2k^{-1}-1}}{Z/n}, k_{\text{w}} = 1 \tag{23}$$

$$\frac{D_2nV_{\text{out}} + (2|\Phi| - D_2)V_{\text{in}}}{4Lf_{\text{sw}}} \geq \frac{nV_{\text{out}}\sqrt{1-2k^{-1}}}{Z/n}, k_{\text{w}} = 0 \tag{24}$$

Based on this inequation system, the following boundary conditions can be derived:

$$D_2 \geq \frac{(2-2|\Phi|)k^{-1} + 4nLf_{\text{sw}}/Z}{1+k^{-1}} \tag{25}$$

$$D_2 \geq \frac{-2|\Phi|k^{-1} + 4nLf_{\text{sw}}/Z}{1-k^{-1}} \tag{26}$$

$$|\Phi| \geq 0.5 - 0.5k^{-1} + \frac{4\sqrt{2}Lf_{\text{sw}}}{Z} \tag{27}$$

III. THE ZVS-OPTIMIZED CONSTANT FREQUENCY MODULATION SCHEME

There are infinite combinations of Φ and $D_{1/2}$ that can operate the DAB converter at a certain operational power, switching frequency, input and output voltage. A construction method is thus needed to guide the selection of the advantageous values of Φ and $D_{1/2}$ for the modulation scheme based on the optimization objectives. A straightforward construction method is proposed based on the full ZVS boundary conditions derived in the last section to construct a ZVS-optimized constant switching frequency modulation scheme. This modulation scheme features continuity of the phase shift values,

meaning no abrupt change of phase shift value will happen during the operation. And full ZVS operation can be achieved in the majority of the operational range.

A. CONSTRUCTION OF THE MODULATION SCHEME

This modulation scheme consists of three regions. The converter will operate in the EPS mode 2 region at high power and in the TPS mode 1 region at low power. An EPS mode 1 region is in between to connect them. To achieve the optimal ZVS performance in the whole range, a straightforward method of constructing the modulation scheme is proposed, in which the values of phase shifts in each region are determined by linear interpolation between two anchor operational points. Compared to using Lagrange multiplier method to minimize current stress [39], this method does not require complex calculation. Thus, it is a simple and effective way to construct ZVS-optimized modulation schemes.

For the EPS mode 2 region, the first anchor point is where the converter's power is maximized. It can be written as (28).

$$\begin{cases} |\Phi| = 0.5 \\ D_1 = 1 \\ D_2 = 1 \end{cases} \tag{28}$$

The other anchor point of the EPS mode 2 region is defined by $\Phi_{\text{EPS2(min)}}$ and $D_{\text{EPS(bdr)}}$. $\Phi_{\text{EPS2(min)}}$ is the minimum value according to (21) or (27) depending on the value of k, and $D_{\text{EPS(bdr)}}$ is the value of D to in the EPS transition mode as shown in Fig. 1(e). Thus, this anchor point can be written as (29).

$$\begin{cases} |\Phi| = \Phi_{\text{EPS2(min)}} \\ D = D_{\text{EPS(bdr)}} = 1 - 2\Phi_{\text{EPS2(min)}} \end{cases} \tag{29}$$

Note that, since it is EPS mode, one of $D_{1/2}$ equals to 1 depending on the value of k, and the non-unity D is calculated according to (29).

With the two anchor points, the non-unity value of $D_{1/2}$ inside the EPS mode 2 region can be calculated based on the value of Φ by linear interpolation by:

$$D_{1/2} = \frac{0.5 + \Phi_{\text{EPS2(min)}}(2|\Phi| - 2)}{0.5 - \Phi_{\text{EPS2(min)}}}, \ \Phi_{\text{EPS2(min)}} < |\Phi| \leq 0.5 \tag{30}$$

The TPS mode 1 region starts at $\Phi = 0$ and ends at $\Phi_{\text{TPS(max)}}$ defined by (9) or (15), at which point either D_1 or D_2 will be equal to 1. With these two anchor Φ values defined for the TPS mode 1, the values of D_1 and D_2 inside the TPS mode 1 can be obtained based on the minimum values to ensure full ZVS operation, which can be calculated based on $|\Phi|$ value and (6) and (7) or (14) and (13).

The EPS mode 1 region bridges these two regions. The values of $D_{1/2}$ can be calculated using linear extrapolation between the two anchor points of the EPS mode 2 and TPS mode 1 regions. The resulting equations for $D_{1/2}$ are shown in (31). $\Phi_{\text{TPS(max)}}$ is the maximum value of $|\Phi|$ to operate in the full ZVS region of TPS mode1, which can be calculated by (9) or (15). $D_{1/2,\text{TPS(max)}}$ is the maximum value of $D_{1/2}$ to operate in the full ZVS region of TPS mode 1, and it can be calculated by substituting $|\Phi|$ with $\Phi_{\text{TPS(max)}}$ in (6) and (7) or (14) and (13).

$$D_{1/2} = \frac{1 - 2\Phi_{\text{EPS(min)}} - D_{1/2,\text{TPS(max)}}}{\Phi_{\text{EPS(min)}} - \Phi_{\text{TPS(max)}}} \left(|\Phi| - \Phi_{\text{TPS(max)}}\right) + D_{1/2,\text{TPS(max)}} \tag{31}$$

Using this construction method, the phase shift values of the constant frequency modulation scheme can be calculated for different k values. Furthermore, by applying the power calculation equation in Table 1, the corresponding power level at each operational point can be calculated. Fig. 2 shows four examples of the constant frequency modulation scheme and the values of phase shift for different values of k. It can be seen that when $k < 1$ and the DAB converter is operating in the BUCK mode, it operates in EPS mode 2 when the power is high and transitions into EPS mode 1 and further into TPS mode 1 when the power level decreases. A special case of the modulation scheme is when k is close to 1, as shown in Fig. 2(c). In this case, the minimum value of $|\Phi|$ required for the full ZVS operation in EPS mode 2 is close to zero based on (21) and (27). This indicates that the converter will operate mostly in EPS mode 2, and will not transition into TPS mode 1. When V_{out} further increases and the DAB converter is in the BOOST mode, the maximum power of the converter can be easily reached with a small value of Φ, meaning the converter might operate mostly in the TPS mode 1 region and transition into EPS mode 1 or EPS mode 2 when the power level is approaching its maximum. In the example of Fig. 2(d) where V_{out} is high, the DAB converter operates in TPS mode 1 in its power range, and at the maximum power, the operation is at the edge between the TPS mode 1 and EPS mode 1 region.

B. LOSS OF ZVS DURING TRANSITION

Even though it is possible for all the switches of the DAB converter to have ZVS when it is operated in the TPS mode 1, EPS mode 1, and EPS mode 2, certain switches will lose the ZVS when the operation is at the boundary between two modes. A straightforward way to explain the loss of ZVS is that, in such boundary regions, the switching actions of the H-bridge I are very close to, or even overlapping, that of the H-bridge II. For the EPS boundary mode illustrated in Fig. 1(c), the switching action of $(v_1 : 0 \rightarrow +V_{\text{in}})$ overlaps that of $(v_2 : -nV_{\text{out}} \rightarrow +nV_{\text{out}})$, and $(v_1 : 0 \rightarrow -V_{\text{in}})$ overlaps that of $(v_2 : +nV_{\text{out}} \rightarrow -nV_{\text{out}})$. It can be seen from Table 3 that the switching action $(v_1 : 0 \rightarrow +V_{\text{in}})$ requires a negative current value for ZVS, while the switching actions $(v_2 : -nV_{\text{out}} \rightarrow +nV_{\text{out}})$ requires a positive current value. Therefore, the ZVS requirement for one of the switching actions can not be fulfilled, and ZVS for certain switches will be lost. Similarly, operating at the edge of the operation region where the switching actions of the two H-bridges are very close will lead to insufficient current values for different ZVS requirements, resulting in partial

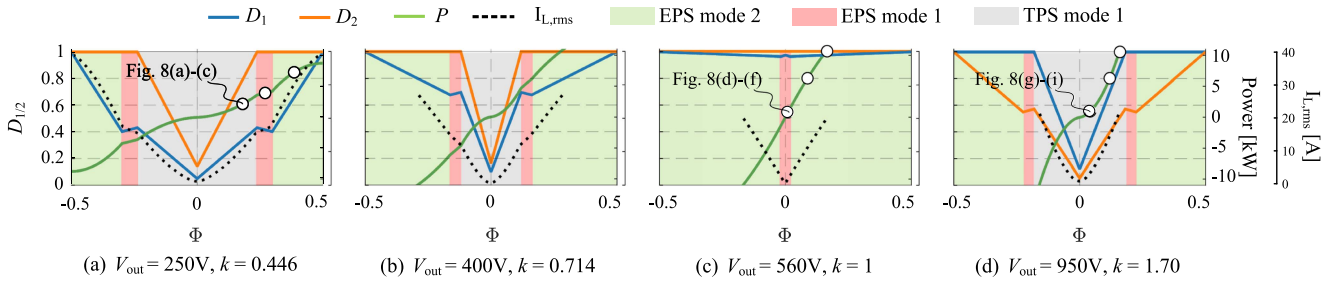

FIGURE 2. The phase shift ($D_{1/2}$ and Φ) and power values for the constant frequency TPS + EPS modulation scheme, under different k values. f_{sw} = 25kHz, and other specifications of the converter can be found in Table 4.

ZVS or even hard switching. Therefore, this proposed constant frequency modulation scheme introduces improvements to the number of ZVS events compared to other modulation methods, but the loss of ZVS for certain transistors during the transition of modulation regions is inevitable.

Based on the method of construction of the modulation scheme, it is clear that the converter is able to operate with full ZVS in the TPS mode 1 region. This is because all the values of $D_{1/2}$ and Φ in this region fulfill the ZVS requirements shown in (6), (7) and (9) or (14), (13),and (15).

However, full ZVS will not always be achieved in the EPS mode region. The reason lies in the choice of the anchor points. As explained in Section III-A, the second anchor point for the EPS mode 2 region is at $|\Phi| = \Phi_{\text{EPS(min)}}$, and $D_{1/2} = 1 - 2\Phi_{\text{EPS(min)}}$. In this operational point, even though the ZVS requirement for Φ as shown in (21) or (27) is fulfilled, the ones for $D_{1/2}$ as written in (19) and (20) or (25) and (26) are not guaranteed. This indicates that 2 or 4 transistors on the primary side might lose ZVS when the operation is close to this anchor point of EPS mode 2 region.

This operational point is still chosen as the anchor point of EPS mode 2 region because the resulting modulation scheme offers better overall ZVS performance in the whole operational range. The alternative anchor point is at $|\Phi| = \Phi_{\text{EPS2(min)}}$ with $D_{1/2} = D_{\text{EPS2(min)}}$ fulfilling the ZVS requirements of (19) and (20) or (25) and (26). With this anchor point, all the operational points inside the EPS mode 2 region will achieve full ZVS. However, part of the resulting operational region that bridges this anchor point to that of the TPS mode 1 can only achieve ZVS on two out of eight transistors.

To explain this phenomenon, the constant frequency modulation scheme at $V_{\text{out}} = 250$ V, k = 0.446 and $f_{\text{sw}} = 25$ kHz?enlrg -10pt?> is shown in Fig. 3 together with the important boundaries of Φ and D. Moreover, the number of switches that can achieve ZVS is also marked in the specific regions. It can be seen that by following the proposed method of scheme construction, the DAB converter will operate with 8/8 ZVS in the whole TPS mode 1 region and most of the EPS mode 2 region, but will operate with 6/8 ZVS in edge of the EPS mode 2 region and the EPS mode 1 region. However, if the alternative anchor point of EPS mode 2 is used, the resulting modulation scheme (indicated by the dashed blue line) will include a specific region inside the EPS mode 2 region where

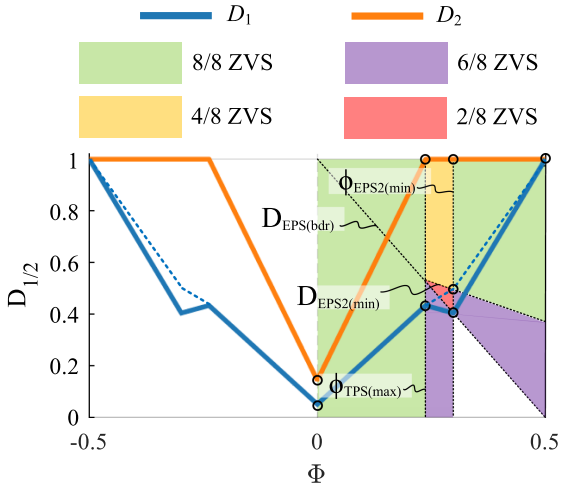

FIGURE 3. Phase shift ($D_{1/2}$ and Φ) values for the constant frequency TPS + EPS modulation scheme when V_{out} = 250 V, k = 0.446, f_{sw} = 25 kHz. Specifications of the converter can be found in Table 4. The blue dashed line shows the alternative scheme when the anchor point of EPS mode 2 is changed.

the only 2/8 transistors can achieve ZVS. Note that it is still possible to achieve partial ZVS for the other six switches.

The loss of ZVS happens not only when the power level changes while k is fixed, but also when k changes and the power level is fixed. Fig. 4 shows the phase shift values at different V_{out} for the constant frequency modulation scheme at the full power operation. When V_{out} is low, the DAB converter needs to operate with high values of Φ and in the EPS mode 2 region to deliver the maximum rated power. However, as V_{out} further increases, the maximum power operational point will shift from EPS mode 2 region into EPS 1. During the transition from EPS mode 2 to EPS mode 1 (700 V < V_{out} < 870 V), the converter will lose ZVS on two transistors during the full power operation according to the calculation based on the ZVS requirements in Table 3. It can be seen that, the loss of ZVS during mode transition can cover a significant operational range as illustrated in Fig. 4. This will bring detrimental impacts on the EMI and efficiency performance of the DAB converter, especially when it is used in the EV charging application due to the reasons explained in the Introduction.

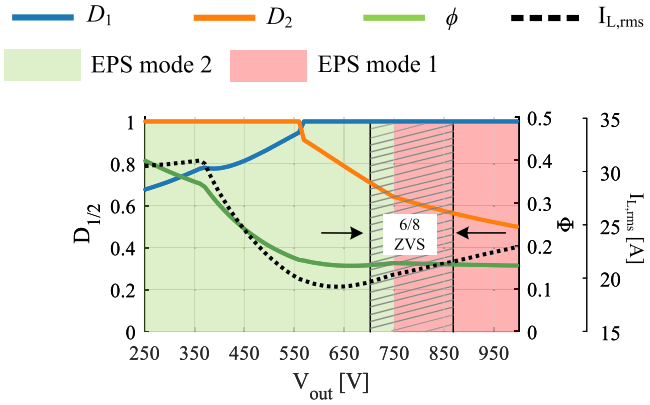

FIGURE 4. Phase shift ($D_{1/2}$ and Φ) values for the constant frequency TPS + EPS modulation scheme at the full power operation, $f_{sw} = 25$kHz. Specifications of the converter can be found in Table 4.

IV. THE VARIABLE FREQUENCY MODULATION SCHEME FOR FULL POWER OPERATION

To prevent the DAB from operating at the edge of the operational regions where certain switches will lose ZVS during full power operation, the phase shift Φ can be increased or decreased so that the operation moves more deeply into ZVS-beneficial regions. However, the operational power of the DAB converter will be changed by changing Φ. Table 1 shows the conditions of D_1, D_2, Φ and the power calculation of the TPS mode 1 and mode 4. It can be seen that the phase shift Φ is a proportional control parameter for the power of the DAB operation. Therefore, it is not possible to maintain ZVS by only changing Φ. To solve this issue, the switching frequency f_{sw} can be utilized.

A. WORKING PRINCIPLE

As can be seen from the equations of power calculation in Table 1, the power is inversely proportional to f_{sw}. Thus, The switching frequency f_{sw} can be utilized as an additional control parameter to shift the operation of the DAB converter to the ZVS-beneficial modulation modes without changing the power level. f_{sw} can either be increased or decreased to help maintain the ZVS performance. The first one is to increase f_{sw} when the DAB converter is about to enter the boundary mode from EPS mode 2, which decreases the output power, requiring an increase in Φ to achieve the same power. As a result, the operation will remain in the EPS mode 2 region where full ZVS can be achieved. Similarly, f_{sw} can be reduced and Φ needs to be reduced to maintain the same power. The lower value of Φ will help to maintain the operation in the full ZVS part of the TPS mode 1 region.

From the ZVS point of view, whether f_{sw} is increased or decreased is inconsequential as long as ZVS is achieved. However, each approach has their pros and cons. In the case of decreasing f_{sw}, the switching losses on the transistors can be mitigated, but the dB/dt and magnetic flux density stress of the transformer core increases. This means the magnetic components must be designed at the lowest switching frequency and most critical flux density to avoid saturation, resulting in the oversizing of magnetic components. Conversely, increasing f_{sw} will amplify the switching losses, but due to lower dB/dt and flux density stress at higher f_{sw} the magnetic components can be designed similarly to those in the conventional constant frequency modulation. Therefore, aside from the EMC filter circuitry, no hardware change is required when f_{sw} is increased, and this maintains the converter's power density and lowers the design complexity. This paper focuses on the case of increasing f_{sw}.

B. CONSTRUCTION OF THE MODULATION SCHEME FOR FULL POWER OPERATION

The variable frequency modulation scheme is modified based on the constant frequency modulation scheme. Since the operation always remains in the EPS mode 2 region in the variable switching frequency modulation scheme, the anchor point of the EPS mode 2 region can be chosen to be the alternative one that fulfills the full ZVS requirements, which is at $|\Phi| = \Phi_{EPS2(min)}$ with $D_{1/2} = D_{EPS2(min)}$. In this way, the EPS mode 2 region is utilized more efficiently.

The value of phase shifts and f_{sw} for the variable switching frequency modulation scheme for full power operation is obtained by iteration on the basis of the constant frequency modulation scheme in full power. Firstly, the constant frequency modulation scheme is constructed with the new anchor point and interpolation method. Secondly, the operational region/ZVS performance of the DAB converter operating at its maximum power in this constant frequency modulation scheme is checked. If the operation is not in the ZVS-beneficial EPS mode 2 region and full ZVS can not be achieved, f_{sw} will be increased by an increment. Then Φ will be increased accordingly and $D_{1/2}$ will be re-calculated based on the construction method for the constant frequency modulation scheme explained in Section III-A with the new f_{sw}. This is done until the same power level before changing f_{sw} is reached. Then, the ZVS requirements will be checked again. If full ZVS is not yet achieved, the previous step will be repeated, and f_{sw} and Φ will be further increased until full ZVS operation is reached. This process is looped through different values of k to cover the whole voltage regulation range.

Fig. 5 shows the resulting variable frequency modulation scheme for full power operation. It can be seen that starting from $V_{out} \approx 700$ V, f_{sw} is increased from 25 kHz to around 50 kHz, allowing the converter to operate with an increased value of Φ compared to Fig. 4. As a result, the full power operation remains in the ZVS-beneficial EPS mode 2 region for the whole output voltage range. This indicates that by using the proposed variable frequency modulation scheme, the DAB converter can always have full ZVS during the full-power operation in the whole output voltage range, which is essential for the EV charging application.

Note that it is possible to extend the variable switching frequency modulation to lower power with the same construction method. In this paper, it is only applied to the full power

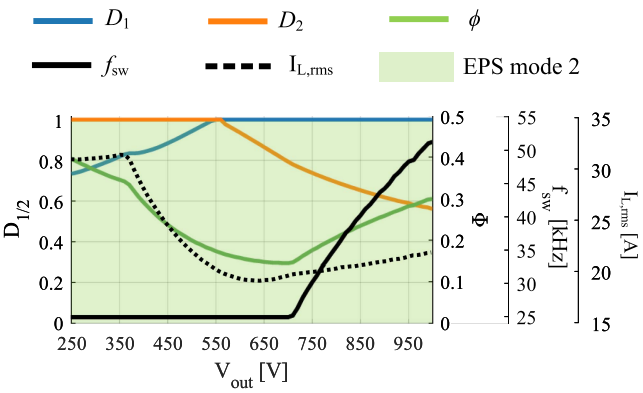

FIGURE 5. Phase shift ($D_{1/2}$ and Φ) and f_{sw} values for the variable frequency modulation scheme at the full power operation. Specifications of the converter can be found in Table 4.

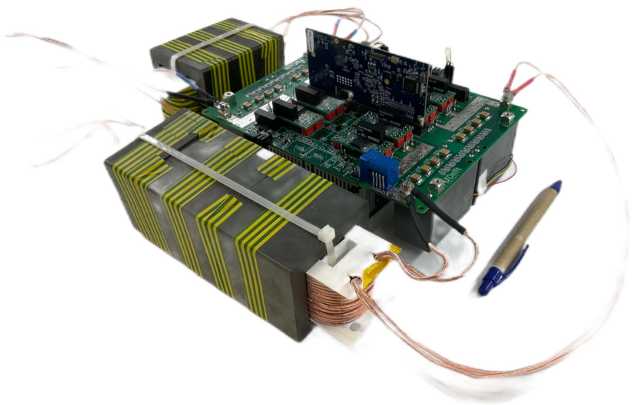

FIGURE 6. Picture of the 11 kW DAB converter prototype.

operation because it is identified as the dominating operational scenario for EV charging.

TABLE 4. The Specification of the DAB Prototype

V_{in} [V]	640
V_{out} [V]	250 - 950
P_{max} [kW]	11
$I_{out(max)}$ [A]	30
Transistor	G3R20MT12K
Litz wire	AWG41 x 600
Transformer core shape	EE70/33/32
Number of stacked cores n_{cores}	5
Number of parallel wires	2
N_{pri}	16
N_{sec}	14
Leakage inductance L_k [μH]	16.2
External inductor core shape	EE70/33/32
Number of stacked cores n_{cores}	3
Number of parallel wires	2
N	9
Inductor airgap [mm]	1.42
Inductance L_{ext} [μH]	87.8

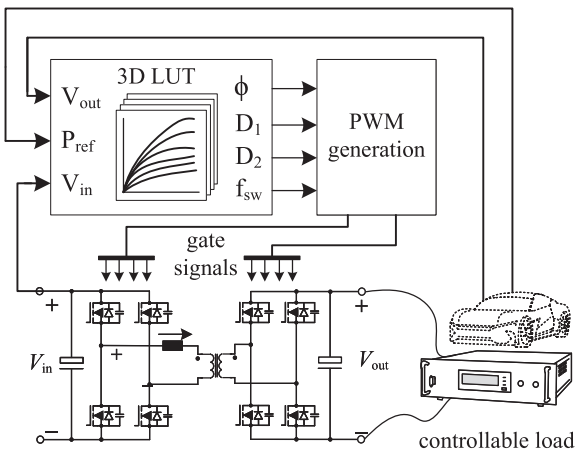

FIGURE 7. Diagram of the lookup table control method.

V. EXPERIMENTAL VERIFICATION

An 11 kW DAB converter prototype is built to verify the ZVS performance of the proposed modulation schemes. This converter features a wide output voltage range from 250 V to 950 V, which ensures its effectiveness in charging both 400 V and 800 V EVs. Fig. 6 shows the DAB prototype. Table 4 summarizes the specification of the DAB prototype.

A lookup table based power control is implemented in the micro-controller TMS320F28379D for the DAB prototype. Fig. 7 shows the control method of the prototype. This method is simple and does not require much computational resources. To generate the required lookup table, a matrix containing the power at a given value of Φ, V_{in} and V_{out} is created in Matlab. This is done with a very high resolution for Φ. For each combination of V_{in} and V_{out}, the power vs Φ curve is sampled at fixed power values using the 1D interpolation function. These values of Φ are then stored in a 3D matrix used in the lookup table to determine Φ based on the converter power reference, V_{in} and V_{out}. The values of D_1 and D_2 are paired with Φ based on the construction of the modulation scheme.

During the charging operation, V_{in} and V_{out} of the DAB converter are measured. Together with the required charging power value P_{ref} sent by the EV, the values of the phase shifts and switching frequency can be extracted from the lookup table. These values are then used to generate the PWM gate signals for the transistors.

A. RESULTS OF CONSTANT FREQUENCY MODULATION SCHEME

Firstly, the constant frequency modulation scheme is tested on the prototype to set up a benchmark of ZVS and efficiency performance. Fig. 8 shows the operational waveform of the DAB converter operated with the constant frequency modulation scheme. These nine waveforms are located in at the operational points shown in Fig. 2.

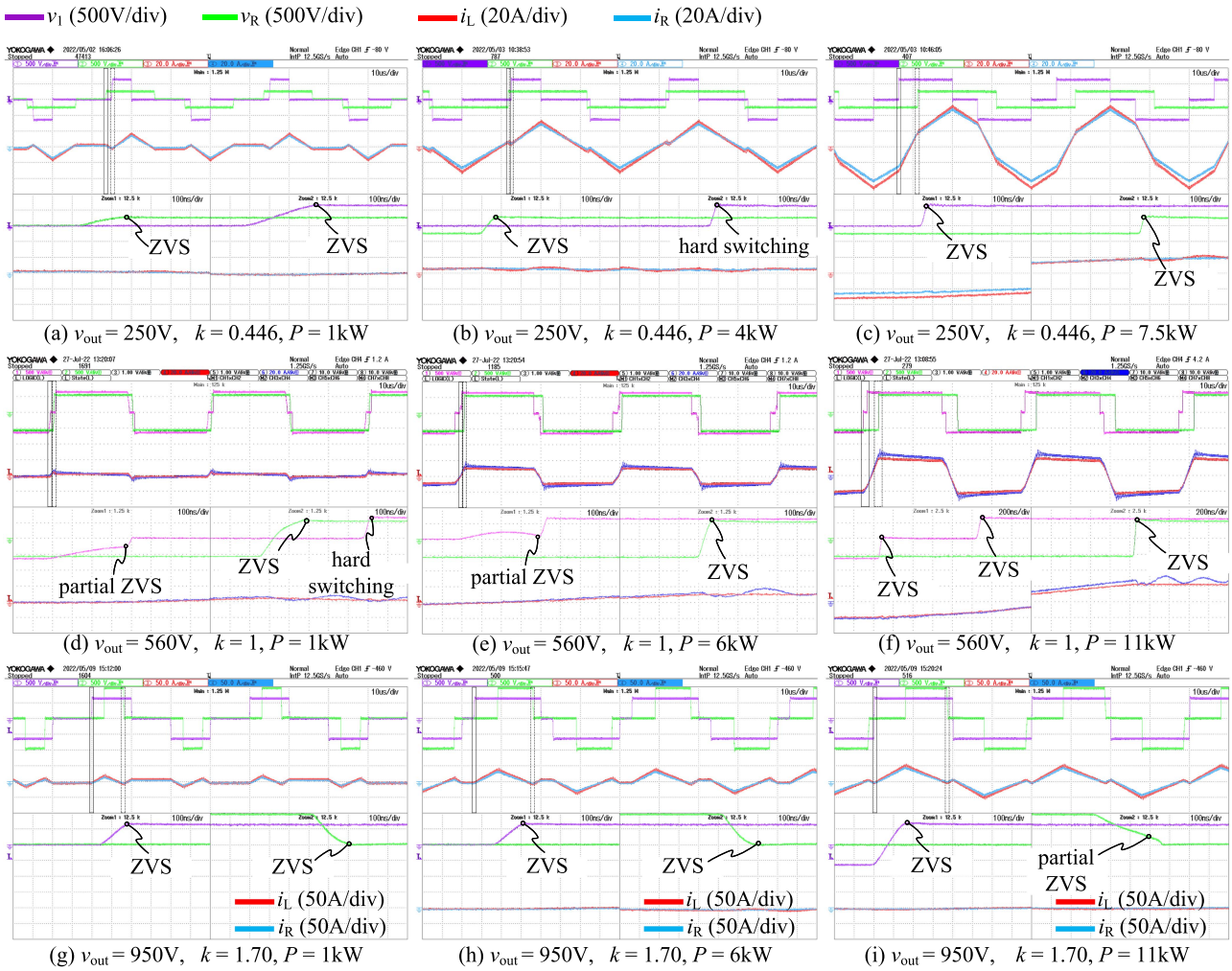

FIGURE 8. Waveform of the DAB converter operating with the proposed constant switching frequency TPS + EPS modulation scheme, with V_{in} = 640 V and f_{sw} = 25 kHz. v_R and i_R are the voltage and current measured from the secondary winding of the transformer.

As can be seen from Fig. 8(a)–(c), the converter transitions from TPS mode 1 to EPS mode 1 and further into EPS mode 2 when the power increases. In Fig. 8(a) and (c), where the converter operates deeply in TPS mode 1 and EPS mode 2, all transistors have ZVS as indicated by the zoom-in waveform of the H-bridge voltage and current. And it can be seen in Fig. 8(b), where the converter operates in EPS mode 1, the $0 \rightarrow +V_{in}$ switching action of the primary side half bridge does not meet the ZVS requirement of having a zero or negative inductor current value. As a result, two transistors on the primary side lose ZVS as indicated by the sharp voltage change of v_1. In comparison, v_R has a slower and smooth change with this small positive value of inductor current, indicating that ZVS is achieved.

As v_{out} increases and k is close to 1, the converter operates only in EPS modes as seen in Fig. 8(d)–(f). In the low power scenario as shown in Fig. 8(d), the converter is operating in the EPS mode 1 and is very close to the EPS transition mode, as the switching action $0 \rightarrow +V_{in}$ occurs closely to the switching action $-V_{out} \rightarrow +V_{out}$. According to the general ZVS equations listed in Table 3, the switching action $-V_{in} \rightarrow 0$ and $0 \rightarrow +V_{in}$ requires a slightly negative i_L to achieve ZVS, but the switching action $-V_{out} \rightarrow V_{out}$ requires zero or positive i_L to achieve ZVS. As a result, only the four transistors on the secondary side achieve ZVS while the four on the primary side cannot, which is indicated by the waveform of v_1 and v_R in Fig. 8(d). When the power increases, the converter operates at the edge of the EPS mode 2. The switching action $0 \rightarrow +V_{in}$ that requires a negative i_L is still close to the switching action $-V_{out} \rightarrow V_{out}$ which requires a positive i_L, leading to the loss of ZVS for the two transistors on the primary side. However, the switching action $-V_{in} \rightarrow 0$ now obtains ZVS due to the sufficiently negative i_L. When the power further increases and the converter operates deeply in the EPS mode 2, full ZVS is achieved as shown in Fig. 8(f).

In the case where V_{out} is high, the converter only operates in the TPS mode 1 and at the edge of the EPS mode 1 region, as it can be seen in Figs. 2 and 8(g)–(i). Full ZVS can be easily achieved when the power level is not high and the converter is operating deeply in the TPS mode 1 region.

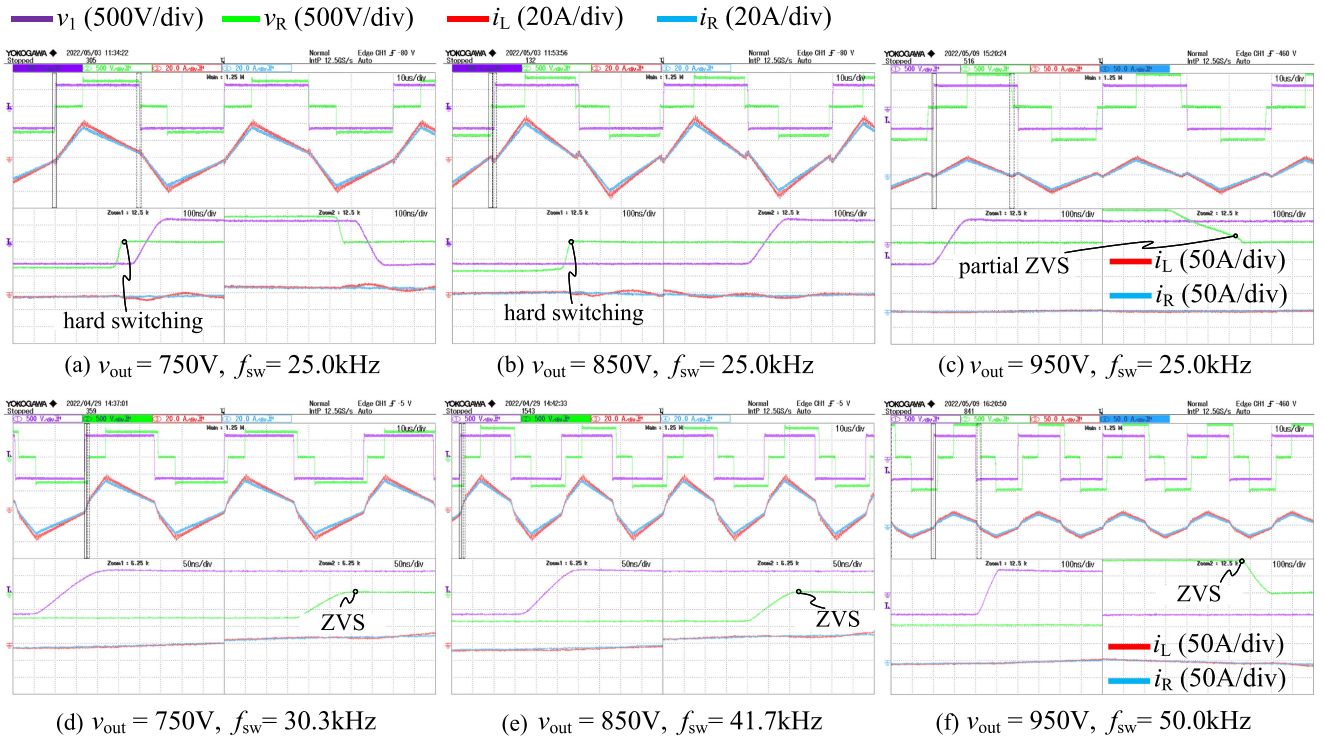

FIGURE 9. Waveform of the DAB converter with the proposed constant modulation scheme (a)-(c), and variable switching frequency modulation scheme (d)-(f), with V_{in} = 640V and P = 11kW (full power). v_R and i_R are the voltage and current measured from the secondary winding of the transformer.

However, as the power increases, the converter moves to the edge of the TPS mode 1 and EPS mode 1, making it challenging to maintain full ZVS performance. As can be seen from Fig. 8(i), the switching action $+V_{out} \rightarrow 0$ occurs very close to $+V_{in} \rightarrow -V_{in}$. The prior one requires a negative current value for ZVS, while the later one requires a zero or positive current. Consequently, the two transistors of the half bridge on the secondary side achieve only partial ZVS as it can be seen in Fig. 8(i).

In summary, the constant frequency modulation scheme operates well, and full ZVS is achieved in the majority of the operational range. However, the loss of ZVS happens when the operation is at the boundary of two modulation regions. In the case of unity voltage gain, 4 out of 8 transistors might lose ZVS, and in other boundary operation cases, 2 out of 8 transistors will lose ZVS. The loss of ZVS during full power operation is also demonstrated.

B. RESULTS OF VARIABLE FREQUENCY MODULATION SCHEME

Fig. 9 shows the waveforms of the DAB converter operating with full power but different output voltage in the constant frequency (Fig. 9(a)–(c)) and variable frequency modulation scheme (Fig. 9(d)–(f)).

It can be seen from Fig. 9(a)–(c) that the converter in the constant frequency modulation scheme need to transition from EPS mode 2 to EPS mode 1 when V_{out} increases during full power operation. This is not beneficial for the ZVS performance because 2 out of 8 transistors will lose ZVS as explained in Section III-B and seen in Fig. 9(a)–(c). In the case of EV charging where the full power operation takes up most of the charging process, the loss of ZVS brought by the constant frequency modulation scheme will have a more significant impact, especially on the EMI performance.

With the variable switching frequency modulation scheme, both f_{sw} and Φ are adjusted so that the operation of the converter is kept in the full ZVS region. As shown in Fig. 9(d)–(f), f_{sw} as well as Φ are increased compared to the constant frequency modulation scheme, moving the operation into the full ZVS EPS mode 2 region. This demonstrates that by using the variable switching frequency modulation scheme, the ZVS performance during the full power operation can be improved compared to the constant frequency modulation scheme.

C. EFFICIENCY PERFORMANCE

The measured efficiency performance of the proposed constant frequency modulation scheme in the whole operational range is shown in Fig. 10. It is evident that the overall efficiency performance is excellent. The converter's efficiency is above 95% in the whole range, and the highest efficiency is measured to be 98.8%. Most importantly, the efficiency performance when operating above 2 kW is well above 97%. This demonstrates that this modulation scheme can provide excellent efficiency performance to the DAB converter for the wide voltage range EV charging application.

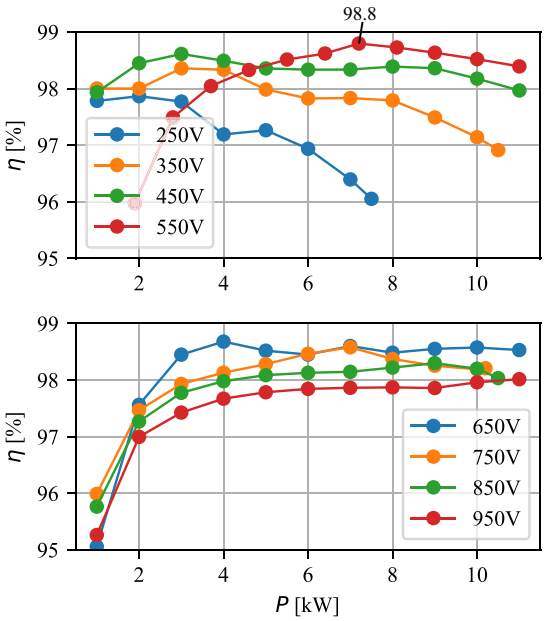

FIGURE 10. Tested efficiency of the constant frequency modulation schemes in the whole operation range.

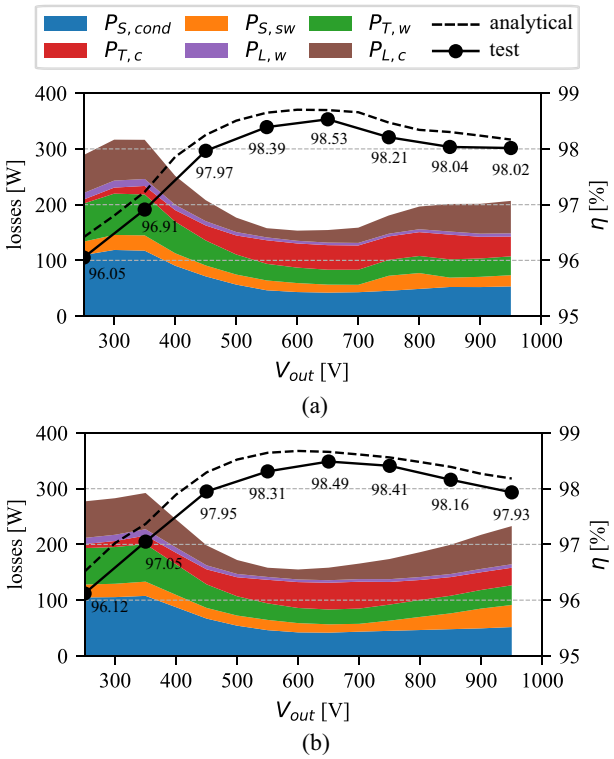

FIGURE 11. Tested efficiency, estimated losses, and estimated efficiency of the constant frequency and variable frequency modulation schemes at full power. (a) constant frequency modulation scheme. (b) variable frequency modulation scheme.

Relatively low efficiency can be observed when operating at very low values of V_{out} and P, and also when V_{out} equals or close to 550 V. For the high power low V_{out} operation, the current stresses during the high power operation are problematic, leading to significant conduction losses and low efficiency performance. For the case when the power is low and V_{out} is high, the high switching losses brought by the high blocking voltage result in the efficiency drop. When V_{out} equals or close to 550 V, the voltage ratio k is close to 1. According to the constructed modulation scheme shown in Fig. 2(c), the converter will lose ZVS during low power operation, which is verified by the test shown in Fig. 8(d). This also contributes to the relatively low efficiency performance.

The efficiency performances of the two modulation schemes at full power operation are compared. Fig. 11 shows the tested efficiency at the full power operation for the constant frequency and variable frequency modulation scheme. To provide more insights into the efficiency performance, the converter's losses and efficiency are also calculated analytically and plotted. The detailed losses calculation models can be found in [50], [51]. As it can be seen from Fig. 11, the estimated efficiency matches well with the testing results. Thus, the estimated loss breakdown can be used to help interpret the efficiency performance.

It can be seen from the tested efficiency that, the variable switching frequency modulation scheme slightly improves the efficiency performance when $V_{\text{out}} > 700$ V. As V_{out} continues to increase, the improvement of efficiency starts to reduce. When V_{out} is as high as 950 V, the efficiency performance of the variable frequency modulation becomes slightly lower than that of the constant frequency one. The reason behind is that, the converter starts to lose ZVS when $V_{\text{out}} > 700$ V (as it can be seen in Fig. 9(a) and (b)), causing the switching losses to increase (as it can be seen from the switching loss $P_{\text{S,sw}}$ stack plot in Fig. 11). Whereas in the variable frequency modulation, by slightly increasing f_{sw}, the ZVS is maintained for all transistors, resulting in lower switching losses overall. As V_{out} continues to increase, the operation moves to the ZVS-beneficial region for the constant frequency scheme, but f_{sw} and $P_{\text{S,sw}}$ continue increasing for the variable frequency scheme. An interesting fact to point out is that, as f_{sw} increases, the transformer core loss $P_{\text{T,c}}$ is reduced due to the lowered flux density stress. This benefits the efficiency performance of the variable frequency scheme. Secondly, the efficiency performances for these two modulation schemes when $V_{\text{out}} < 700$ V are different. This is mainly due to the different choices of the anchor point for the EPS mode 2 region, whose reason and details are presented in Section III-B.

Overall, Based on the tested efficiency, the average efficiency in full power operation for the constant frequency and variable frequency modulation schemes can be calculated to be 97.76% and 97.80%, respectively. This demonstrates that by adopting the variable frequency modulation scheme, not only full ZVS can be maintained for the whole voltage regulation range, but also the efficiency performance will not be sacrificed for the full power operation.

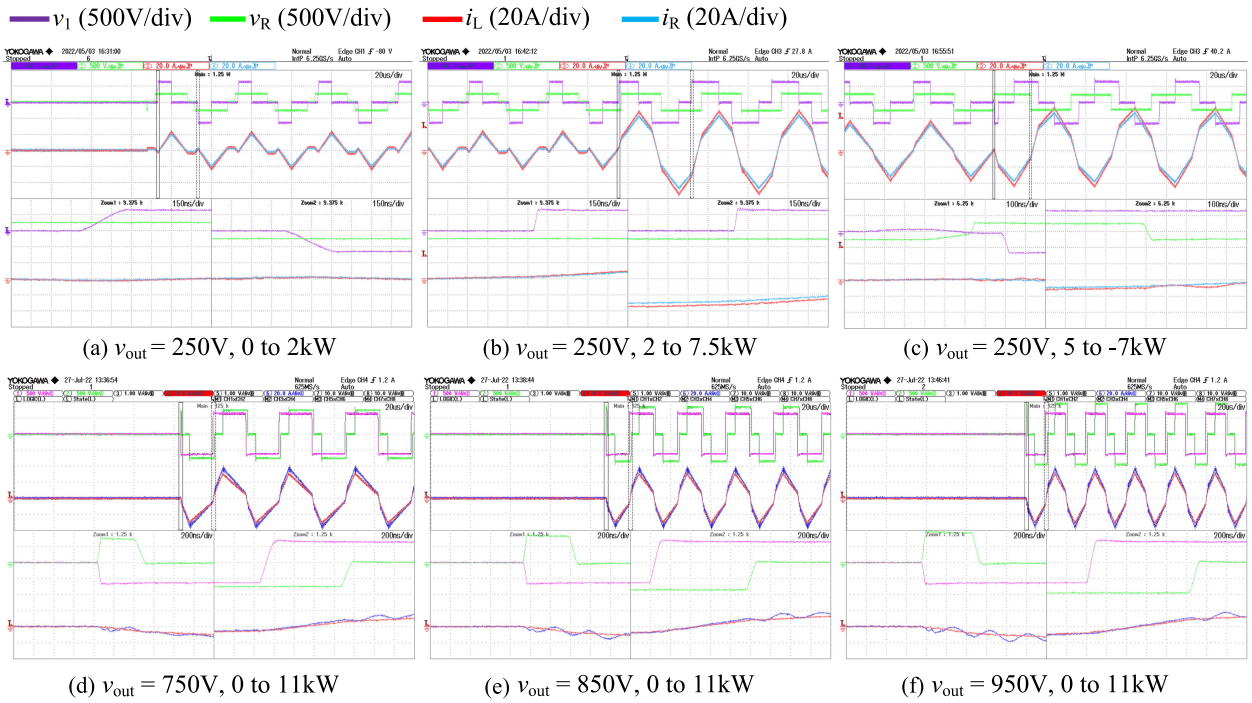

FIGURE 12. Waveform of transient behaviours of the DAB converter with the proposed constant frequency modulation scheme (a)–(c), and variable switching frequency modulation scheme (d)–(f), with V_{in} = 640V. v_R and i_R are the voltage and current measured from the secondary winding of the transformer.

D. TRANSIENT BEHAVIOURS

Fig. 12 shows the waveform of load change transient behaviours of the DAB prototype. It can be seen that, the PWM gate signal of the converter can be quickly adjusted in response to the load change. No obvious current and voltage overshoot and offset are introduced during the transient. It is worth mentioning that, the sudden load change from positive power (grid to vehicle) to negative power (vehicle to grid) as shown in Fig. 12(c) will not happen in real scenarios. Moreover, the sudden output voltage change won't be an issue in EV charging because the EV battery voltage changes continuously and slowly during a charging session.

VI. CONCLUSION

The ZVS-optimized constant and variable switching frequency modulation schemes proposed for the DAB converter aim to enhance ZVS performance in EV charging applications while concurrently maintaining high efficiency. These schemes are formulated based on ZVS boundary conditions, ensuring ease of implementation.

Contrary to existing modulation schemes that focus on optimizing current stress, the proposed constant switching frequency scheme excels in achieving extensive ZVS operation across a wide voltage regulation range, ensuring ZVS on all eight transistors for the majority of the operational span. Nonetheless, this paper acknowledges the inevitable ZVS loss on two or four transistors during the modulation method transitions in the constant switching frequency modulation scheme, presenting challenges for EMI and efficiency.

To address this challenge, the paper introduces a variable switching frequency modulation scheme and outlines its construction methodology. The essence of this approach lies in the dynamic adjustment of the switching frequency to strategically steer the converter's operation into ZVS-favorable regions whenever ZVS is jeopardized. This dynamic approach ensures that ZVS is maintained for all transistors. Given that power modules predominantly operate at full capacity in EV charging scenarios, this variable switching frequency scheme is specifically designed for full-power operation in this study.

Experimental testing on an 11 kW, 250V-950 V DAB prototype validates the efficacy of the proposed modulation schemes. The ZVS performances are verified for both modulation schemes. The extensive ZVS range of the constant switching frequency modulation scheme and the loss of ZVS during mode transitions are illustrated. The full ZVS operation of the variable switching frequency modulation scheme is also demonstrated for full power operation. The efficiency performances of both modulation schemes are presented, demonstrating successful improvement of ZVS performance while maintaining excellent efficiency.

The results of this study provide substantial evidence supporting the feasibility and effectiveness of the proposed modulation schemes. These findings indicate that the proposed modulation schemes are promising solutions for enhancing the performance and reliability of DAB converters in the context of wide voltage range EV charging applications.

REFERENCES

[1] R. W. DeDoncker, M. H. Kheraluwala, and D. M. Divan, "Power conversion apparatus for DC/DC conversion using dual active bridges," U.S. Patent5,027,264, Jun. 25, 1991. Accessed: Oct. 3, 2023. [Online]. Available: https://patents.google.com/patent/US5027264A/en

[2] R. W. A. A. De Doncker, D. M. Divan, and M. H. Kheraluwala, "A three-phase soft-switched high-power-density DC/DC converter for high-power applications," *IEEE Trans. Ind. Appl.*, 27, no. 1, pp. 63–73, Feb. 1991.

[3] M. N. Kheraluwala, R. W. Gascoigne, D. M. Divan, and E. D. Baumann, "Performance characterization of a high-power dual active bridge DC-to-DC converter," *IEEE Trans. Ind. Appl.*, vol. 28, no. 6, pp. 1294–1301, Nov./Dec. 1992.

[4] F. Krismer, S. Round, and J. W. Kolar, "Performance optimization of a high current dual active bridge with a wide operating voltage range," in *Proc. IEEE 37th Power Electron. Specialists Conf.*, 2006, 1–7.

[5] G. G. Oggier, R. Leidhold, G. O. Garcia, A. R. Oliva, J. C. Balda, and F. Barlow, "Extending the ZVS operating range of dual active bridge high-power DC-DC converters," in *Proc. IEEE 37th Power Electron. Specialists Conf.*, 2006, pp. 1–7.

[6] G. G. Oggier, G. O. GarcÍa, and A. R. Oliva, "Switching control strategy to minimize dual active bridge converter losses," *IEEE Trans. Power Electron.*, vol. 24, no. 7, pp. 1826–1838, Jul. 2009.

[7] H. Bai and C. Mi, "Eliminate reactive power and increase system efficiency of isolated bidirectional dual-active-bridge DC–DC converters using novel dual-phase-shift control," *IEEE Trans. Power Electron.*, vol. 23, no. 6, pp. 2905–2914, Nov. 2008.

[8] H. Zhou and Ashwin M. Khambadkone, "Hybrid modulation for dual active bridge bi-directional converter with extended power range for ultracapacitor application," in *Proc. IEEE Indust. Appl. Soc. Annu. Meeting*, 2008, pp. 1–8.

[9] Y. Wang, S. W. H. de Haan, and J. A. Ferreira, "Optimal operating ranges of three modulation methods in dual active bridge converters," in *Proc. IEEE 6th Int. Power Electron. Motion Control Conf.*,2009, pp. 1397–1401.

[10] G. Guidi, M. Pavlovsky, A. Kawamura, T. Imakubo, and Y. Sasaki, "Improvement of light load efficiency of dual active bridge DC-DC converter by using dual leakage transformer and variable frequency," in *Proc. IEEE Energy Convers. Congr. Expo.*, 2010, pp. 830–837.

[11] A. K. Jain and R. Ayyanar, "PWM control of dual active bridge: Comprehensive analysis and experimental verification," *IEEE Trans. Power Electron.*, vol. 26, no. 4, pp. 1215–1227, Apr. 2011.

[12] G. Oggier, G. O. García, and A. R. Oliva, "Modulation strategy to operate the dual active bridge DC-DC converter under soft switching in the whole operating range," *IEEE Trans. Power Electron.*, vol. 26, no. 4, pp. 1228–1236, Apr. 2011.

[13] F. Krismer and J. W. Kolar, "Closed form solution for minimum conduction loss modulation of DAB converters," *IEEE Trans. Power Electron.*, vol. 27, no. 1, pp. 174–188, Jan. 2012.

[14] B. Zhao, Q. Song, and W. Liu, "Power characterization of isolated bidirectional dual-active-bridge DC–DC converter with dual-phase-shift control," *IEEE Trans. Power Electron.*, vol. 27, no. 9, pp. 4172–4176, Sep. 2012.

[15] X. Li and Y.-F. Li, "An optimized phase-shift modulation for fast transient response in a dual-active-bridge converter," *IEEE Trans. Power Electron.*, vol. 29, no. 6, pp. 2661–2665, Jun. 2014.

[16] G. G. Oggier, M. Ordonez, J. M. Galvez, and F. Luchino, "Fast transient boundary control and steady-state operation of the dual active bridge converter using the natural switching surface," *IEEE Trans. Power Electron.*, vol. 29, no. 2, pp. 946–957, Feb. 2014.

[17] X.-F. He, Z. Zhang, Y.-Y. Cai, and Y.-F. Liu, "A variable switching frequency hybrid control for ZVS dual active bridge converters to achieve high efficiency in wide load range," in *Proc. IEEE Appl. Power Electron. Conf. Expo.*, 2014, pp. 1095–1099.

[18] J. Hiltunen, V. Väisänen, R. Juntunen, and P. Silventoinen, "Variable-frequency phase shift modulation of a dual active bridge converter," *IEEE Trans. Power Electron.*, vol. 30, no. 12, pp. 7138–7148, Dec. 2015.

[19] J. Huang, Y. Wang, Z. Li, and W. Lei, "Unified triple-phase-shift control to minimize current stress and achieve full soft-switching of isolated bidirectional DC–DC converter," *IEEE Trans. Ind. Electron.*, vol. 63, no. 7, pp. 4169–4179, Jul. 2016.

[20] X. Han, Y. Tan, and H. Ma, "The switching frequency optimization of dual phase shift control for dual active bridge DC-DC converter," in *Proc. IEEE 43rd IECON Annu. Conf. Indust. Electron. Soc.*, 2017, pp. 1610–1615.

[21] P. He and A. Khaligh, "Comprehensive analyses and comparison of 1 kW isolated DC–DC converters for bidirectional EV charging systems," *IEEE Trans. Transport. Electrific.*, vol. 3, no. 1, pp. 147–156, Mar. 2017.

[22] Z. Qin, Y. Shen, P. C. Loh, H. Wang, and F. Blaabjerg, "A dual active bridge converter with an extended high-efficiency range by DC blocking capacitor voltage control," *IEEE Trans. Power Electron.*, vol. 33, no. 7, pp. 5949–5966, Jul. 2018.

[23] L. Zhu, A. R. Taylor, G. Liu, and K. Bai, "A multiple-phase-shift control for a SiC-based EV charger to optimize the light-load efficiency, current stress, and power quality," *IEEE Trans. Emerg. Sel. Topics Power Electron.*, vol. 6, no. 4, pp. 2262–2272, Dec. 2018.

[24] Q. Gu, L. Yuan, J. Nie, J. Sun, and Z. Zhao, "Current stress minimization of dual-active-bridge DC–DC converter within the whole operating range," *IEEE Trans. Emerg. Sel. Topics Power Electron.*, vol. 7, no. 1, pp. 129–142, Mar. 2019.

[25] L. Jin, B. Liu, and S. Duan, "ZVS soft switching operation range analysis of three-level dual-active bridge DC–DC converter under phase shift control strategy," *IEEE Trans. Ind. Appl.*, vol. 55, no. 2, pp. 1963–1972, Mar./Apr. 2019.

[26] S. Shao, M. Jiang, W. Ye, Y. Li, J. Zhang, and K. Sheng, "Optimal phase-shift control to minimize reactive power for a dual active bridge DC–DC converter," *IEEE Trans. Power Electron.*, vol. 34, no. 10, pp. 10193–10205, Oct. 2019.

[27] S. A. Assadi, H. Matsumoto, M. Moshirvaziri, M. Nasr, M. S. Zaman, and O. Trescases, "Active saturation mitigation in high-density dual-active-bridge DC–DC converter for on-board EV charger applications," *IEEE Trans. Power Electron.*, vol. 35, no. 4, pp. 4376–4387, Apr. 2020.

[28] Y. Yan, H. Bai, A. Foote, and W. Wang, "Securing full-power-range zero-voltage switching in both steady-state and transient operations for a dual-active-bridge-based bidirectional electric vehicle charger," *IEEE Trans. Power Electron.*, vol. 35, no. 7, pp. 7506–7519, Jul. 2020.

[29] F. Zahin, A. Abasian, and S. A. Khajehoddin, "An alternative dual active bridge modulation to minimize RMS current and extend ZVS range," in *Proc. IEEE Energy Convers. Congr. Expo.*, 2020, pp. 5952–5959.

[30] N. Noroozi, A. Emadi, and M. Narimani, "Performance evaluation of modulation techniques in single-phase dual active bridge converters," *IEEE Open J. Indust. Electron. Soc.*, vol. 2, pp. 410–427, 2021.

[31] G. Xu, L. Li, X. Chen, Y. Liu, Y. Sun, and M. Su, "Optimized EPS control to achieve full load range ZVS with seamless transition for dual active bridge converters," *IEEE Trans. Ind. Electron.*, vol. 68, no. 9, pp. 8379–8390, Sep. 2021.

[32] G. Xu, L. Li, X. Chen, W. Xiong, X. Liang, and M. Su, "Decoupled EPS control utilizing magnetizing current to achieve full load range ZVS for dual active bridge converters," *IEEE Trans. Ind. Electron.*, vol. 69, no. 5, pp. 4801–4813, May 2022.

[33] L. Li, G. Xu, W. Xiong, D. Liu, and M. Su, "An optimized DPS control for dual-active-bridge converters to secure full-load-range ZVS with low current stress," *IEEE Trans. Transport. Electrific.*, vol. 8, no. 1, pp. 1389–1400, Mar. 2022.

[34] J. Hu, S. Cui, and R. W. De Doncker, "Natural boundary transition and inherent dynamic control of a hybrid-mode-modulated dual-active-bridge converter," *IEEE Trans. Power Electron.*, vol. 37, no. 4, pp. 3865–3877, Apr. 2022.

[35] L. Gong et al., "A dynamic ZVS-guaranteed and seamless-mode-transition modulation scheme for the DAB converter that maximizes the ZVS range and lowers the inductor RMS current," *IEEE Trans. Power Electron.*, vol. 37, no. 11, pp. 13119–13134, Nov. 2022.

[36] A. Tong, L. Hang, G. Li, X. Jiang, and S. Gao, "Modeling and analysis of dual-active-bridge isolated bidirectional DC/DC converter to minimize RMS current," *IEEE Trans. Power Electron.*, vol. 33, no. 6, pp. 5302–5316, Jun. 2018.

[37] D. Mou et al., "Optimal asymmetric duty modulation to minimize inductor peak-to-peak current for dual active bridge DC–DC converter," *IEEE Trans. Power Electron.*, vol. 36, no. 4, pp. 4572–4584, Apr. 2021.

[38] D. Mou, Q. Luo, J. Li, Y. Wei, and P. Sun, "Five-degree-of-freedom modulation scheme for dual active bridge DC–DC converter," *IEEE Trans. Power Electron.*, vol. 36, no. 9, pp. 10584–10601, Sep. 2021.

[39] Z. Guo, "Modulation scheme of dual active bridge converter for seamless transitions in multiworking modes compromising ZVS and conduction loss," *IEEE Trans. Ind. Electron.*, vol. 67, no. 9, pp. 7399–7409, Sep. 2020.
[40] G. Xu, L. Li, X. Chen, Y. Liu, Y. Sun, and M. Su, "Optimized EPS control to achieve full load range ZVS with seamless transition for dual active bridge converters," *IEEE Trans. Ind. Electron.*, vol. 68, no. 9, pp. 8379–8390, Sep. 2021.
[41] "Global EV Outlook," 2023. [Online]. Available: https://www.iea.org/reports/global-ev-outlook-2023
[42] "Charging with a Tesla," 2023. [Online]. Available: https://support.fastned.nl/hc/en-gb/articles/360012178313-Charging-with-a-Tesla-Model-3
[43] "Charging with a Mercedes-Benz," 2023. [Online]. Available: https://support.fastned.nl/hc/en-gb/articles/360009674054-Mercedes-Benz,
[44] "Charging with an Audi," 2023. [Online]. Available: https://support.fastned.nl/hc/en-gb/articles/360000815988-Audi
[45] D. Lyu, T. B. Soeiro, and P. Bauer, "Impacts of different charging strategies on the electric vehicle battery charger circuit using phase-shift full-bridge converter," in *Proc. IEEE 19th Int. Power Electron. Motion Control Conf.*, 2021, pp. 256–263.
[46] "Charging with a Porsche," 2022. [Online]. Available: https://support.fastned.nl/hc/en-gb/articles/360039667693-Porsche
[47] "Charging with a Citroën," 2022. [Online]. Available: https://support.fastned.nl/hc/en-gb/articles/215884498-Citro
[48] "Charging with a Kia," 2023. [Online]. Available: https://support.fastned.nl/hc/en-gb/articles/4408899202193-Kia
[49] "Charging with a Hyundai," 2022. [Online]. Available: https://support.fastned.nl/hc/en-gb/articles/4405121276945
[50] D. Lyu, T. B. Soeiro, and P. Bauer, "Multi-objective design and benchmark of wide voltage range phase-shift full bridge DC/DC converters for ev charging application," *IEEE Trans. Transport. Electrific.*, to be published, doi: 10.1109/TTE.2023.3254203.
[51] J. Muhlethaler, "Modeling and multi-objective optimization of inductive power components," Ph.D. thesis, ETH, Zurich, Switzerland, 2012.

DINGSIHAO LYU (Graduate Student Member, IEEE) received the B.Sc. degree in electrical engineering from the University of Electronic Science and Technology of China, Chengdu, China, in 2017, and the M.Sc. degree in electrical power engineering from the Delft University of Technology, Delft, The Netherlands, in 2019. He is currently working toward the Ph.D. degree in electrical engineering with DCES Group (dc systems, energy conversion, and storage), Delft University of Technology. His research interests include uni/bi-directional DC/DC power electronic converters and multi-objective design of power electronic converters.

COEN STRAATHOF received the B.Sc. degree in electrical engineering and the M.Sc. degree in electrical power engineering from the Delft University of Technology, Delft, The Netherlands, in 2019 and 2022, respectively. He is currently an Electical Engineer with EST-Floattech, designing battery management systems for the maritime industry.

THIAGO BATISTA SOEIRO (Senior Member, IEEE) received the B.Sc. (with Hons.) and M.Sc. degrees in electrical engineering from the Federal University of Santa Catarina, Florianopolis, Brazil, in 2004 and 2007, respectively, and the Ph.D. degree from the Swiss Federal Institute of Technology, Zurich, Switzerland, in 2012. During the Master and Ph.D. studies, he was a Visiting Scholar with the Power Electronics and Energy Research Group, Concordia University, Montreal, QC, Canada, and with the Center for Power Electronics Systems, Blacksburg, VA, USA, respectively. From 2012 to 2013, he was a Researcher with the Power Electronics Institute, Federal University of Santa Catarina. From 2013 to 2018, he was with the Corporate Research Center, ABB Switzerland Ltd., Baden-Dattwil, Switzerland, where he was a Senior Scientist. From 2018 to 2022, he was with the DC Systems, Energy Conversion and Storage Group, Delft University of Technology, Delft, The Netherlands, where he was also an Associate Professor. From January 2022 to October 2022, he was with the Power Management and Distribution Section (TEC-EPM) for the European Space Research and Technology Centre, Noordwijk, The Netherlands. Since October 2022, he has been a Full Professor with Power Electronics with the Power Electronics and EMC Group , University of Twente, Enschede, The Netherlands. His research interests include advanced high power converters and dc system integration. Dr. Soeiro was the recipient of the 2013 IEEE Industrial Electronics Society Best Conference Paper Award and the Best Paper awards in the International Conference on Power Electronics (ECCE Asia 2011), International Conference on Industrial Technology (ICIT 2013), Conference on Power Electronics and Applications EPE15 (ECCE Europe 2015), and International Conference on Power Electronics and Motion Control 2020 and 2022 (PEMC 2020 and 2022).

ZIAN QIN (Senior Member, IEEE) received the B.Eng. degree in electrical engineering from Beihang University, Beijing, China, in 2009, the M.Eng. degree in electrical engineering from the Beijing Institute of Technology, Beijing, China, in 2012, and the Ph.D. degree in electrical engineering from Aalborg University, Aalborg, Denmark, in 2015. He is currently an Assistant Professor with the Delft University of Technology, Delft, The Netherlands. In 2014, he was a Visiting Scientist with Aachen University, Aachen, Germany. He has authored more than 100 journals/conference papers, four book chapters, two international patents, and also several European and Dutch national projects in his research field, which include power quality and stability of power electronics-based grid, and solid state transformers.

He is also an Associate Editor for IEEE TRANS INDUSTRIAL ELECTRONICS, and a Guest Associate Editor for IEEE JOURNAL OF EMERGING AND SELECTED TOPICS and IEEE TRANS ENERGY CONVERSION. He is a Distinguished Reviewer for 2020 of IEEE TRANSACTIONS OF INDUSTRIAL ELECTRONICS. He was the Technical Program Chair of IEEE-PEDG 2023, IEEE-ISIE 2020, and IEEECOMPEL 2020.

PAVOL BAUER (Senior Member, IEEE) received the master's degree in electrical engineering from the Technical University of Kosice, Koice, Slovakia, in 1985, and the Ph.D. degree from the Delft University of Technology, Delft, The Netherlands, in 1995. He is currently a Full Professor with the Department of Electrical Sustainable Energy, Delft University of Technology and the Head of DC Systems, Energy Conversion and Storage Group. He is also a Professor with the Brno University of Technology, Brno, Czech Republic, and a Honorary Professor with Politehnica University Timisoara, Timisoara, Romania. From 2002 to 2003, he was with KEMA (DNVGL, Arnhem) on different projects related to power electronics applications in power systems. He has authored or coauthored more than 120 journal and 500 conference papers (with H factor Google scholar 40,Web of Science 26). He is also the author or co-author of eight books, holds seven international patents and organized several tutorials at the international conferences. His research interests mainly include power electronics for charging of electric vehicles and DC grids. He has worked on many projects for industry concerning wind and wave energy, power electronic applications for power systems, such as Smarttrafo and HVDC systems, projects for smart cities, such as PV charging of electric vehicles, PV and storage integration, contactless charging, and participated in several Leonardo da Vinci, H2020 and Electric Mobility Europe EU Projects as Project partner (ELINA, INETELE, E-Pragmatic, Micact, Trolley 2.0, OSCD, P2P, Progressus) and a Coordinator (PEMCWebLab.com-Edipe, SustEner, Eranet DCMICRO). He is the former Chairman of Benelux IEEE Joint Industry Applications Society, Power Electronics and Power Engineering Society chapter, Chairman of the Power Electronics and Motion Control (PEMC) council, Member of the Executive Committee of European Power Electronics Association (EPE), and also the Member of international steering committee at numerous conferences.